Thermodynamic and Electronic Properties of OsB_2 from First-Principles Calculations

Y. Cheng[a,b], J.-W. Yang[a], Y.-X. Wang[a], G.-F. Ji[c] and X.-R. Chen[a,*]

[a]College of Physical Science and Technology, Sichuan University, Chengdu 610064, China

[b]School of Electrical, Computer and Energy Engineering, Arizona State University, AZ 85287-5706, USA

[c]Laboratory for Shock Wave and Detonation Physics Research, Institute of Fluid Physics
Chinese Academy of Engineering Physics, Mianyang 621900, China

(Received April 9, 2013; in final form January 26, 2014)

The pressure induced phase transitions of OsB_2 from the orthorhombic structure (Orth) to the hexagonal structure (Hex) is investigated by using *ab initio* plane-wave pseudopotential density functional theory, together with quasi-harmonic Debye model. We find that the pressure-induced phase transition occurs at 2.8 GPa and 12.5 GPa by local density approximation and general gradient approximation, respectively. It is predicted that OsB_2 has no phase transition temperature from the Orth structure to the Hex structure. Moreover, the dependences of the relative volume V/V_0 on the pressure, thermal expansion coefficient α on the pressure and temperature are also successfully obtained. The electronic properties including energy band, total and partial density of states and electron density difference for two structures are also analyzed. The Mulliken charges and Bond populations for both Orth and Hex structures are also obtained.

DOI: 10.12693/APhysPolA.125.1186

PACS: 71.15.Mb, 61.50.Ks, 67.25.de, 71.20.−b

1. Introduction

As a member of metal diborides, OsB_2 has been reported to be superconductor with $T_c = 2.1$ K early in 1975 [1]. Chen et al. [2] calculated the structural and electronic properties of OsB_2 using density functional theory with or without taking into account the spin–orbit (SO) interaction. They indicated that the good metallicity and hardness of OsB_2 might suggest its potential application as hard conductors. Chiodo et al. [3] obtained the electronic structural properties of OsB_2 using the projector augmented-wave (PAW) method. Moreover, Hao et al. [4] investigated the elastic anisotropic of OsB_2, indicating that OsB_2 possesses high elastic anisotropy at zero temperature and zero pressure. Hebbache et al. [5] showed that OsB_2 was a new superhard material and has a metallic character.

However, Gou et al. [6] indicated that OsB_2 is an incompressible material, but not a superhard material. Chen et al. [7] investigated the roles of bond topology and covalency in the phase stability and elastic strength of $5d$ transition-metal diborides, focusing on elements (M = W, Re, Os) by the PAW potential. They noted that the pressure-induced phase transition for OsB_2 from orthorhombic structure (Orth: space group $Pmmn$) to ReB_2-type hexagonal structure (Hex: space group $P6_3/mmc$) occurs at 2.5 GPa.

More recently, we have investigated the structure, elastic properties and elastic anisotropy of orthorhombic OsB_2 under pressure in the frame of the generalized gradient approximation (GGA) as well as local density approximation (LDA) [8]. Our results showed that the elastic constants, bulk modulus and Debye temperature of OsB_2 tend to increase with increasing pressure, and OsB_2 is not a superhard material.

In this work, we here make first-principles calculations to investigate the structural phase transition of OsB_2 from the Orth structure to the Hex structure by using the plane-wave pseudopotential density-functional theory (DFT) through the Cambridge Serial Total Energy Package (CASTEP) program [9, 10] and the quasi-harmonic Debye model [11]. In Sect. 2, we outline the theoretical framework. A detailed description and analysis of our results are displayed in Sect. 3. Finally, a conclusion of the present study is given.

2. Theoretical method

In our calculations, the ultrasoft pseudopotential introduced by Vanderbilt [12] employed for all the ion–electron interaction together with the exchange and correlation functional were treated by local density approximation (LDA-CAPZ) [13] and the generalized gradient approximation (GGA-PBE) [14] as an exchange-correlation function. Pseudo-atomic calculations are performed for Os ($5d^66s^2$) and B ($2s^22p^1$). A plane-wave basis set with an energy cut-off of 400 eV is applied for two structures. In the Brillouin-zone sampling, we use $5 \times 9 \times 6$ and $10 \times 10 \times 4$ k-point Monkhorst–Pack meshes for Orth structure and Hex structure, respectively. The self-consistent calculations were considered to be converged when the total energy of the system was stable within 10^{-6} eV/atom. The Brodyden–

*corresponding author; e-mail: xrchen@scu.edu.cn

Fletcher–Goldfarb–Shanno (BFGS) minimization scheme [15] was used in geometry optimization. The tolerances are set as the difference in total energy being within 10^{-5} eV/atom, the maximum ionic Hellmann–Feynman force within 0.03 eV/Å, the maximum ionic displacement within 0.001 Å, and the maximum stress within 0.05 GPa. These parameters are carefully tested. It is found that these parameters are sufficient in leading to well-converged total energy and elastic constants calculations.

3. Results and discussion

For the Orth and Hex structures of OsB_2 a series of unit cell volumes V (from $0.68V_0$ to $1.64V_0$ for the Orth structure and from $0.64V_0'$ to $1.74V_0'$ for the Hex structure, respectively, where V_0 and V_0' are the equilibrium unit cell volume at zero pressure for Orth and Hex, respectively) are set to obtain the energy–volume data. The calculated E–V points are then fitted to the Vinet equation of state (EOS) [16].

TABLE I

Lattice parameters a, b, c (Å), equilibrium primitive cell volume V (Å^3), bulk modulus B_0 and its pressure derivative B_0' for the Orth and Hex structures of OsB_2 at 0 GPa and 0 K, together with the experimental data and other theoretical results.

	a	b	c	V	u	B_0	B_0'
Orth structure							
LDA (present)	4.628	2.838	4.039	53.055		357.34	4.13
GGA (present)	4.688	2.878	4.088	55.145		327.96	4.17
LDA and APW+lo [2]	4.6433	2.8467	4.4032			365	
LDA+SO and APW+lo [2]	4.6581	2.8700	4.0560			364	
LDA and PP [3]	4.648	2.846	4.047	53.646		364.87	4.1
experiments [18, 19]	4.684	2.872	4.076	54.83			
experiment [17]						365–395	1.4–4
Hex structure							
LDA (present)	2.89		7.251	52.45	0.052	364.05	4.15
GGA (present)	2.93		7.329	54.48	0.052	333.46	4.19

The obtained lattice constant, bulk modulus B_0 and its pressure derivative B_0' for the Orth and the Hex structures of OsB_2 at zero pressure are listed in Table I. For the Orth structure of OsB_2 the equilibrium lattice parameters obtained are in good agreement with the experimental data [17, 18] and other theoretical results [2, 3]. The LDA calculations underestimate the lattice constants, while the GGA calculations overestimate the lattice constants. The bulk modulus B_0 and its pressure derivative B_0' are close with the calculated results [2, 3] as well as the experimental data [19]. Moreover, it is seen that the structural parameters obtained from the GGA calculations for the Orth structure OsB_2 are found to be somewhat in better agreement with the experimental data and other theoretical values than those from the LDA calculations.

For the Hex structure of OsB_2, there exists an internal parameter u, which is a third structural degree of freedom parallel to the c axis. Unfortunately, there are no experimental and theoretical data for our comparison. Throughout similar calculations, we find that the total energy of the Orth structure OsB_2 ($E = -5377.76$ eV in LDA, $E = -5364.59$ eV in GGA) is a little lower than that of the Hex structure OsB_2 ($E = -5377.75$ eV in LDA, $E = -5364.54$ eV in GGA) at zero pressure, implying that the Orth structure OsB_2 maybe more stable than the Hex structure OsB_2 at zero pressure.

A theoretical estimate of the zero-temperature phase transition pressure of OsB_2 between the Orth structure and the Hex structure can be obtained by the Gibbs free energy. In the quasi-harmonic Debye model [11], which had been applied to investigate the thermodynamic properties and the transition pressure of some materials [20–25], the Gibbs free energy is expressed as: $G(V,P,T) = E(V) + PV + A_{\rm vib}(V,T)$, where E is the internal energy, P is the pressure, V is the volume, $A_{\rm vib}$ is the vibrational Helmholtz free energy. When the temperature is zero, the Gibbs free energy equals the enthalpy (i.e., $H(V,P) = E(V) + PV$).

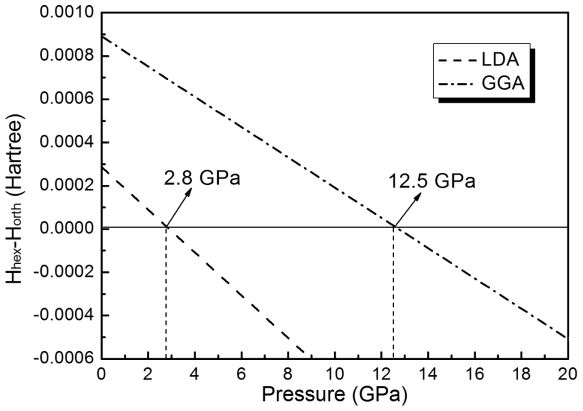

Fig. 1. Pressure-dependent relative enthalpies of OsB_2 in the Orth and Hex structures, where the solid line at zero represents the enthalpy of OsB_2 in the Orth structure.

In Fig. 1, we show the relative enthalpy as a function of pressure. It is found that the phase transition pressure of OsB_2 from the Orth structure to the Hex structure is 2.8 GPa and 12.5 GPa by LDA and GGA, respectively. The LDA result is in good agreement with the value, 2.5 GPa, obtained by Chen et al. [7], who performed their calculation by the projector augmented wave method, and the GGA result is somewhat much larger than that by Chen et al. [7]. Unfortunately, there is no experimental phase transition pressure for our comparison. Thus, in the following, we only present the LDA results of OsB_2 in both the Orth structure and the Hex structure.

In Fig. 2, we illustrate the dependences of calculated normalized volume V/V_0 (V_0 is the zero pressure equilibrium primitive cell volume) on pressure P at a given temperature for the Orth and the Hex structures. It is seen

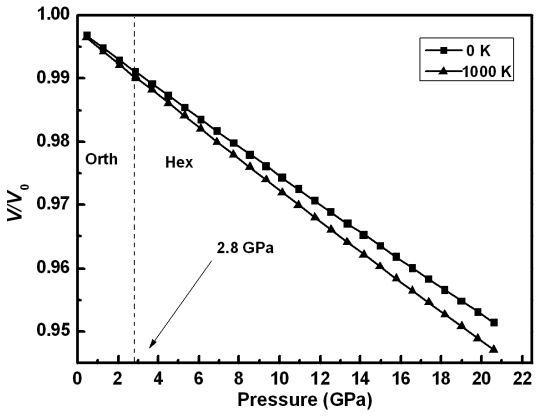

Fig. 2. Normalized primitive cell volume V/V_0 as a function of pressure P for OsB_2 in the Orth and Hex structure at 0 K and 1000 K.

that as pressure P increases, the relative volume V/V_0 decreases at a given temperature. The values of relative volume V/V_0 at higher temperatures are smaller than those at lower temperatures at the same pressure. In addition, the relative volume V/V_0 of the Orth structure becomes 0.99091 and the Hex structure becomes 0.99108 at the transition pressure at zero temperature.

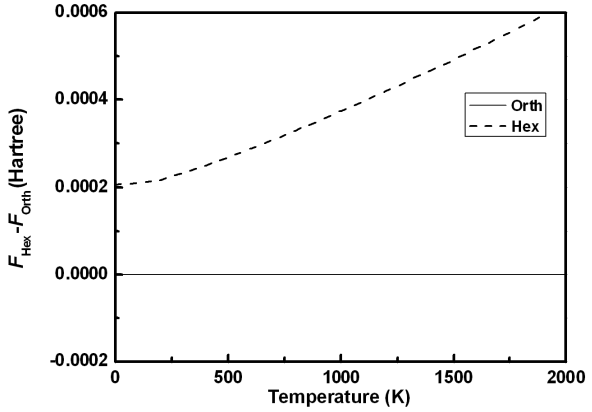

Fig. 3. Temperature-dependent relative Helmholtz free energies of OsB_2 in the Orth and Hex structures at 0 GPa.

In Fig. 3, we present the transition temperatures between the Orth and the Hex structures. When the pressure is zero, the Gibbs free energy G^* equals the Helmholtz free energy F ($F = E + A_{\rm vib}$), we show the variations of the calculated Helmholtz free energies $F_{\rm Orth}$ and $F_{\rm Hex}$ with temperature T at 0 GPa in Fig. 3. We can see two lines detach gradually while the temperature varies from 0 K to 2000 K. Thus, we predict that OsB_2 from the Orth structure to the Hex structure has no transition temperature at 0 GPa.

The temperature and pressure dependences of the thermal expansion coefficient α of OsB_2 in the Orth and Hex structures are indicated in Fig. 4. As the pressure

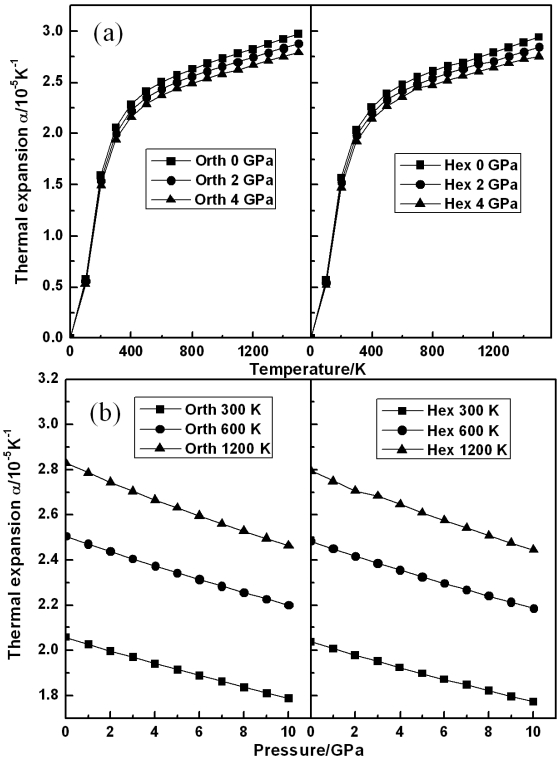

Fig. 4. Variation in thermal expansion coefficient with temperature (a) and pressure (b) for OsB_2 in the Orth and the Hex structures.

increases, the thermal expansion coefficient α decreases (Fig. 4a). The effect of pressure on the thermal expansion coefficient α is very small at low temperatures, but as temperature increases, the effect becomes prominent. We note that the thermal expansion coefficient increases with T^3 at low temperatures and gradually turns into almost a linear increase at high temperatures. The curves for 300, 600, and 1200 K seem parallel to each others (Fig. 4b). Thermal expansion coefficient α decreases almost linearly as the pressure increases. The effect of high temperature on the thermal expansion coefficient α is smaller than the effect of low temperatures. We also found that the orthorhombic structure and hexagonal structure are almost the same sensitive to temperature.

To understand the mechanical properties of the material, the band structures are also calculated for the Orth and Hex structures of OsB_2. We note that there are several bands crossing the Fermi level and some bands crossing each other, which are shown in Fig. 5. These bands are still rather dispersive in the whole Brillouin zone. It evidently exhibits good electronic mobility, indicating the good metallic. The bands show the high symmetry along symmetry point (G) for the Hex structure.

We also display the total density of states (DOS) and the partial density of states (PDOS) of OsB_2 near the Fermi level to elucidate the origin of properties in Fig. 6, where the vertical broken line is the Fermi level $E_{\rm F}$. The

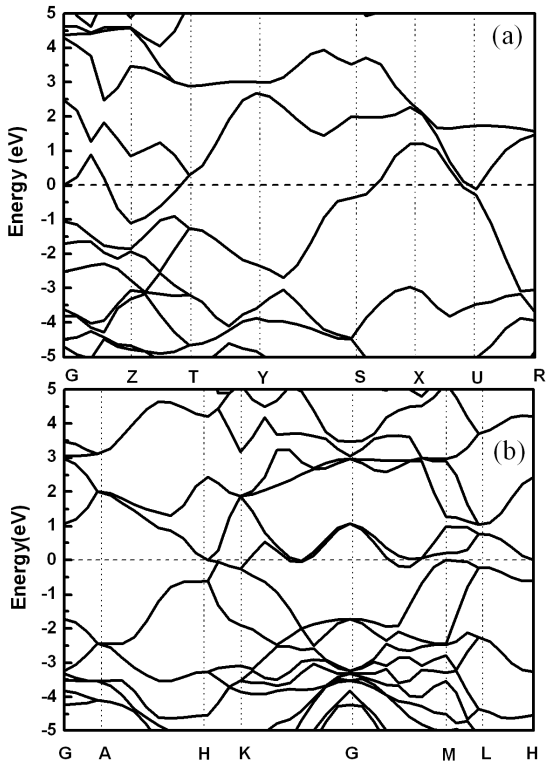

Fig. 5. Band structures of OsB_2 in the Orth (a) and Hex (b) structures.

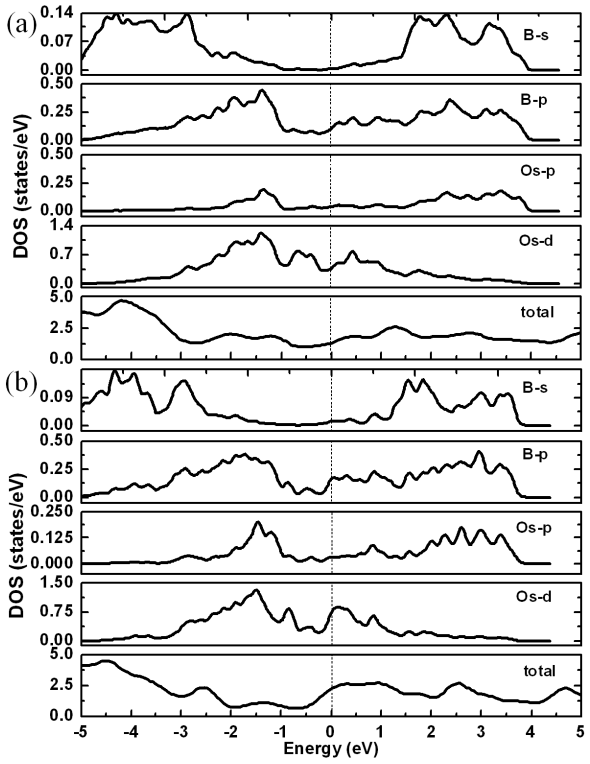

Fig. 6. Total and partial density of states of OsB_2 in the Orth (a) and Hex (b) structures, where broken line at zero is the Fermi level.

PDOS are the p and d electrons of Os atom together with the s and p electrons of B atom. The features are depicted as follows: there are high DOS near the Fermi level; moreover, the B-p states and Os-d states contribute more to the DOS at the Fermi level, while with a rather small contribution from the Os-p and B-s states. This strong hybridization of Os-d and B-p indicates to the strong covalent bonding of Os–B. This bond covalence is responsible for increasing hardness of these compounds. There is a deep valley near the Fermi level. It is the strong hybridization that produces the deep valley and leads to a separation of the bonding states [26]. The presence of deep valley indicates the covalent bonding in the Orth and Hex structures, showing that both structures are stable.

TABLE II

Mulliken charges of species of OsB_2.

Species (Orth)	Total	Charge (e)	Species (Hex)	Total	Charge (e)
B	3.30	−0.30	B	3.32	−0.32
Os	15.40	0.60	Os	15.37	0.63

TABLE III

Bond populations of OsB_2.

Bond (Orth)	Bond popula-tion	Bond length [Å]	Bond (Hex)	Bond popula-tion	Bond length [Å]
B3–B4	0.57	1.79290			
B1–B2	0.57	1.79290	B2–B4	1.89	1.82951
B2–B4	1.12	1.87707	B1–B3	1.89	1.82951
B1–B3	1.12	1.87707	B1–Os1	−0.26	2.18964
B1–Os1	0.09	2.15074	B4–Os2	−0.26	2.18964
B4–Os2	0.09	2.15074	B3–Os2	−0.26	2.18964
B3–Os2	0.09	2.15074	B2–Os1	−0.26	2.18964
B2–Os1	0.09	2.15074	B2–Os2	0.69	2.20152
B2–Os2	0.46	2.17564	B3–Os1	0.69	2.20152
B3–Os1	0.46	2.17564	B1–Os2	0.69	2.20152
B1–Os2	0.46	2.17564	B4–Os1	0.69	2.20152
B4–Os1	0.46	2.17564	B2–B3	−0.11	2.87449
B2–B3	−0.45	2.93406	B1–B4	−0.11	2.87449
B1–B4	−0.45	2.93406			
Os1–Os2	−0.40	2.98543			

Finally, we have calculated the Mulliken charges and bond populations for both Orth and Hex structures because this helps to understand bonding behavior. From Table II, we can note that the charges transfer from Os to B is about 0.6 and 0.63 electrons for OsB_2 in the Orth and Hex structures, respectively, suggesting that the Hex structure has stronger interatomic interaction than the Orth structure. The bond populations indicate the overlap degree of the electron cloud of two bonding atoms [27]. The highest and the lowest values imply that chemical bonds exhibit covalent or ionic bonding. Positive and negative values indicate bonding and antibonding states, respectively. A value for the overlap popula-

tions close to zero indicates that there is no significant interaction between the electronic populations of the two atoms. Bond populations of OsB_2 have been shown in Table III. The bond populations of B2–B4 and B1–B3 change largely, so we mainly discuss the bond populations of B2–B4 and B1–B3. When OsB_2 transfers from the Orth to Hex structures, the B2–B4 and B1–B3 bond lengths decrease from 1.87707 Å to 1.82951 Å, and the bond populations increase from 1.12 to 1.89. This can be easily understood that more electron clouds overlap together, indicating strongly hybridization between both B atoms. This may be due to the Hex volume smaller than the Orth volume when the phase transition occurs as if OsB_2 is compressed. The strongly hybridization may suggest that Hex structure of OsB_2 is more stable than Orth structure.

4. Summary

We have investigated the phase transition of OsB_2 from the Orth structure to the Hex structure by using the *ab initio* plane-wave pseudopotential density functional theory, together with quasi-harmonic Debye model. It is found that the phase transition occurs at 2.8 GPa and 12.5 GPa by LDA and GGA, respectively. We predict that there exists no phase transition temperature for OsB_2 from the Orth structure to the Hex structure. We have also obtained the dependences of the relative volume V/V_0 on the pressure, thermal expansion coefficient α on the pressure and temperature successfully. Through analysis of energy band, both the Orth and Hex structures show good electronic mobility. A detailed study of the total and partial density of states and electron density difference reveals the features of strong covalent B–B and Os–B bonding in the Orth and Hex structures. Through Mulliken charges and bond populations calculated for both Orth and Hex structures, it is seen that the Hex structure is more hybridized than the Orth structure, as is consistent with our analysis of electron density difference.

Acknowledgments

The authors would like to thank the support by the National Natural Science Foundation of China under grant Nos. 11174214 and 11204192, the Defense Industrial Technology Development Program of China under grant No. B1520110002, the National Key Laboratory Fund for Shock Wave and Detonation Physics Research of the China Academy of Engineering Physics under grant No. 2012-Zhuan-08, and the Science and Technology Development Foundation of China Academy of Engineering Physics under grant Nos. 2012A0201007 and 2013B0101002. We also acknowledge the support for the computational resources by the State Key Laboratory of Polymer Materials Engineering of China in Sichuan University.

References

[1] J.M. Vandenberg, B.T. Matthias, E. Corenzwit, H. Barz, *Mater. Res. Bull.* **10**, 889 (1975).

[2] Z.Y. Chen, H.J. Xiang, J.L. Yang, J.G. Hou, Q.S. Zhu, *Phys. Rev. B* **74**, 012102 (2006).

[3] S. Chiodo, H.J. Gotsis, N. Russo, E. Sicilia, *Chem. Phys. Lett.* **425**, 311 (2006).

[4] X.F. Hao, Y.H. Xu, Z.J. Wu, D.F. Zhou, X.J. Liu, J. Meng, *J. Alloys Comp.* **453**, 413 (2008).

[5] M. Hebbache, L. Stuparević, D. Živković, *Solid State Commun.* **139**, 227 (2006).

[6] H.Y. Gou, L. Hou, J.W. Zhang, H. Li, G.F. Sun, F.M. Gao, *Appl. Phys. Lett.* **88**, 221904 (2006).

[7] X.Q. Chen, C.L. Fu, M. Krčmar, G.S. Painter, *Phys. Rev. Lett.* **100**, 196403 (2008).

[8] J.W. Yang, X.R. Chen, F. Luo, G.F. Ji, *Physica B* **404**, 3608 (2009).

[9] M.C. Payne, M.P. Teter, D.C. Allen, T.A. Arias, J.D. Joannopoulos, *Rev. Mod. Phys.* **64**, 1045 (1992).

[10] V. Milman, B. Winkler, J.A. White, C.J. Packard, M.C. Payne, E.V. Akhmatskaya, R.H. Nobes, *Int. J. Quantum Chem.* **77**, 895 (2000).

[11] E. Francisco, M.A. Blanco, G. Sanjurjo, *Phys. Rev. B* **63**, 094107 (2001).

[12] D. Vanderbilt, *Phys. Rev. B* **41**, 7892 (1990).

[13] D.M. Ceperley, B.J. Alder, *Phys. Rev. Lett.* **45**, 566 (1980).

[14] J.P. Perdew, K. Burke, M. Ernzerhof, *Phys. Rev. Lett.* **77**, 3865 (1996).

[15] B.G. Pfrommer, M. Côté, S.G. Louie, M.L. Cohen, *J. Comp. Physiol.* **131**, 233 (1997).

[16] P. Vinet, J.H. Rose, J. Ferrante, J.R. Smith, *J. Phys., Condens. Matter.* **1**, 1941 (1989).

[17] B. Aronsson, *Acta Chem. Scand.* **17**, 2036 (1963).

[18] R.B. Roof, Jr., C.P. Kempter, *J. Chem. Phys.* **37**, 1473 (1962).

[19] R.W. Cumberland, M.B. Weinberger, J.J. Gilman, S.M. Clark, S.H. Tolbert, R.B. Kaner, *J. Am. Chem. Soc.* **127**, 7264 (2005).

[20] X.F. Li, X.R. Chen, C.M. Meng, G.F. Ji, *Solid State Commun.* **139**, 197 (2006).

[21] X.R. Chen, X.F. Li, L.C. Cai, J. Zhu, *Solid State Commun.* **139**, 246 (2006).

[22] Q. Ai, Z.J. Fu, Y. Cheng, X.R. Chen, *Chin. Phys. B* **17**, 2639 (2008).

[23] M.Y. Duan, J.J. Tan, G.F. Ji, X.R. Chen, J. Zhu, *Acta Phys. Pol. A* **118**, 652 (2010).

[24] B. Kong, B. Zhu, Y. Cheng, *Physica B* **406**, 3003 (2011).

[25] X.L. Yuan, D.Q. Wei, Y. Cheng, G.F. Ji, Q.M. Zhang, Z.Z. Gong, *Comp. Mater. Sci.* **58**, 125 (2012).

[26] P. Vajeeston, P. Ravindran, C. Ravi, R. Asokamani, *Phys. Rev. B* **63**, 045115 (2001).

[27] J. Sun, X.F. Zhou, Y.X. Fan, J. Chen, H.T. Wang, *Phys. Rev. B* **73**, 045108 (2006).